

Ion Charge States in a Time-Dependent Wave-Turbulence-Driven Model of the Solar Wind

Roberto Lionello¹  · Cooper Downs¹ · Jon A. Linker¹ · Zoran Mikić¹ · John Raymond² · Chengcai Shen² · Marco Velli³

Received: 28 September 2018 / Accepted: 11 January 2019 / Published online: 29 January 2019
© Springer Nature B.V. 2019

Abstract Ion fractional charge states, measured *in situ* in the heliosphere, depend on the properties of the plasma in the inner corona. As the ions travel outward in the solar wind and the electron density drops, the charge states remain essentially unaltered or “frozen in”. Thus they can provide a powerful constraint on heating models of the corona and acceleration of the solar wind. We have implemented non-equilibrium ionization calculations into a 1D wave-turbulence-driven (WTD) hydrodynamic solar wind model and compared modeled charge states with the *Ulysses* 1994–1995 *in situ* measurements. We have found that modeled charge-state ratios of C^{6+}/C^{5+} and O^{7+}/O^{6+} , among others, were too low compared with *Ulysses* measurements. However, a heuristic reduction of the plasma flow speed has been able to bring the modeled results in line with observations, though other ideas have been proposed to address this discrepancy. We discuss implications of our results and the prospect of including ion charge-state calculations into our 3D MHD model of the inner heliosphere.

Keywords Solar wind · Fractional charge states

1. Introduction

Fractional charge states of ions in the solar corona are determined by the local properties of the plasma. However, the rapidly decreasing electron density of the plasma released into the

This article belongs to the Topical Collection:
Solar Wind at the Dawn of the Parker Solar Probe and Solar Orbiter Era
Guest Editors: Giovanni Lapenta and Andrei Zhukov

✉ R. Lionello
lionel@predsci.com

¹ Predictive Science Inc., 9990 Mesa Rim Rd. Suite 170, San Diego, CA 92121, USA

² Harvard-Smithsonian Center for Astrophysics, 60 Garden St., Cambridge, MA 02138, USA

³ Earth, Planetary, and Space Sciences, UCLA, 595 Charles Young Dr. E., Box 951567, Los Angeles, CA 90095, USA

solar wind prevents further ionization and recombination beyond a few solar radii (Bochsler, 2002; Cranmer, 2002, and references therein). Thus measurements of charge states in the heliosphere such as those performed by *Ulysses*/SWICS (Zurbuchen *et al.*, 2002) give us information and constraints on the properties of the corona from which they originate, the higher-ionization states being associated with hotter regions. While ionization equilibrium is a valid assumption in many cases and especially in the lower corona, it does not apply when the dynamic time scales of the plasma are shorter than those of ionization and recombination. In those instances charge states must be calculated with a time-dependent scheme (Shen *et al.*, 2015), which is then relaxed to a steady state for the steady solar wind solutions computed here. Although the evolution of the charge-state distribution in the solar wind has been studied with sophisticated multi-fluid models (Buergi and Geiss, 1986; Esser, Edgar, and Brickhouse, 1998; Ko *et al.*, 1999; Chen, Esser, and Hu, 2003; Byhring *et al.*, 2011), connecting *in situ* measurements with coronal spectroscopic data still remains problematic (Landi *et al.*, 2014). This very difficulty makes the reproduction of charge states in MHD computational models of the solar corona a robust constraint for the validation of the models themselves. Oran *et al.* (2015) pioneered in this effort by using an external code to evaluate charge states in the solar wind calculation obtained with the Alfvén Wave Solar Model (AWSOM), and comparing them with *in situ* measurements from *Ulysses*. Recently, we incorporated a wave-turbulence-driven (WTD) formulation for coronal heating and solar wind acceleration by Alfvénic turbulence into a 3D MHD model of the global solar corona (Mikić *et al.*, 2018). In this effort, we constrained the model by forward modeling EUV, X-ray, and white-light coronal emission and comparing directly to observations. Although it is our long-term goal to use the calculation of fractional charge states to further constrain our 3D model, it is expedient to start this process with our 1D solar wind model, since it contains analogous heating and acceleration schemes (Lionello *et al.*, 2014b,a). With this aim in mind, we have added the fractional charge-state module of Shen *et al.* (2015) to our 1D model. Then we have compared the calculated C^{6+}/C^{5+} and O^{7+}/O^{6+} ratios and the average iron charge state, $\langle Q \rangle Fe$ with those measured by *Ulysses* during 1994–1995, when the spacecraft spanned a large latitudinal interval. Since our preliminary results could not match the *in situ* data, we have developed and validated a heuristic method to correct the 1D model and improve the comparison with satellite measurements. This modification can also be implemented in 3D calculations. This paper is organized as follows: in Section 2 we describe the 1D model; the first results, the modifications to the model, and the corrected results are in Section 3; we draw our conclusions in Section 4.

2. Model Description

We use the 1D hydrodynamic (HD) model of the solar wind of Lionello *et al.* (2014b,a), which is based on our WTD formulation. This formulation uses the propagation, reflection, and non-linear dissipation of Alfvénic turbulence to heat and accelerate the solar wind (Verdini *et al.*, 2010). This model solves the following set of time-dependent, 1D HD equations:

$$\frac{\partial \rho}{\partial t} = -\frac{1}{A} \frac{\partial}{\partial s} (AU\rho), \quad (1)$$

$$\rho \frac{\partial U}{\partial t} = -\rho U \frac{\partial U}{\partial s} - \frac{\partial}{\partial s} (p + p_w) + g_s \rho + R_s + \frac{1}{s^2} \frac{\partial}{\partial s} \left(s^2 \nu \rho \frac{\partial U}{\partial s} \right), \quad (2)$$

$$\frac{\partial T}{\partial t} = -U \frac{\partial T}{\partial s} - (\gamma - 1) \left[T \frac{1}{A} \frac{\partial}{\partial s} AU - \frac{m_p}{2k\rho} \left(\frac{1}{A} \frac{\partial}{\partial s} Aq - n_e n_p Q(T) + H \right) \right], \quad (3)$$

$$\frac{\partial z_{\pm}}{\partial t} = -[U \pm V_a] \frac{\partial z_{\pm}}{\partial s} - \frac{1}{2}[U \mp V_a] \left(\frac{\partial \log V_a}{\partial s} \frac{\partial \log A}{\partial s} \right) z_{\pm} + \frac{1}{2}[U \mp V_a] \frac{\partial \log V_a}{\partial s} z_{\mp} - \frac{|z_{\mp}|z_{\pm}}{2\lambda_{\odot}\sqrt{A/A_{\odot}}}, \tag{4}$$

$$H = \rho \frac{|z_-|z_+^2 + |z_+|z_-^2}{4\lambda_{\odot}\sqrt{A/A_{\odot}}}, \tag{5}$$

$$p = 2nkT, \tag{6}$$

$$p_w = \frac{1}{2}\rho \frac{(z_- - z_+)^2}{8}, \tag{7}$$

$$R_s = \rho z_+ z_- \frac{\partial \log A}{\partial s}, \tag{8}$$

where $s \geq R_{\odot}$ is the distance along a magnetic field line; p , T , U , and ρ , are the plasma pressure, temperature, velocity, and density. The number density, n , is assumed to be equal for protons (n_p) and electrons (n_e). k is Boltzmann constant. $g_s = g_0 R_{\odot}^2 \hat{\mathbf{b}} \cdot \hat{\mathbf{r}}/r^2$ is the gravitational acceleration parallel to the magnetic field line ($\hat{\mathbf{b}}$). The kinematic viscosity is ν . $A(s) = 1/B(s)$ is the area factor along the field line and the inverse of the magnetic field magnitude $B(s)$. The field aligned component of the vector divergence of the MHD Reynolds stress, $\mathbf{R} = (\delta\mathbf{b}\delta\mathbf{b}/4\pi - \rho\delta\mathbf{u}\delta\mathbf{u})$, is R_s . $\delta\mathbf{u}$ and $\delta\mathbf{b}$ are respectively the fluctuations of the velocity $\mathbf{u} = U(s)\hat{\mathbf{b}} + \delta\mathbf{u}$ and of the magnetic field, $\mathbf{B} = B(s)\hat{\mathbf{b}} + \delta\mathbf{b}$, with $\hat{\mathbf{b}} \cdot \delta\mathbf{b} = 0 = \hat{\mathbf{b}} \cdot \delta\mathbf{u}$. $p_w = \delta\mathbf{b}^2/8\pi$ is the wave pressure. In Equation 3, the polytropic index is $\gamma = 5/3$. The radiation loss function $Q(T)$ is as in Athay (1986). For the heat flux q , according to the radial distance, either a collisional (Spitzer’s law) or collisionless form (Hollweg, 1978) is employed. At a distance of 10 R_{\odot} from the Sun, a smooth transition between the two forms occurs (Mikić *et al.*, 1999). In Equation 4, the Elsasser variables $z_{\pm} = \delta\mathbf{u} \mp \delta\mathbf{b}/\sqrt{4\pi\rho}$ (Dmitruk, Milano, and Matthaeus, 2001) are advanced. z_+ represents an outward-propagating perturbation along a radially outward magnetic field line, while z_- is directed inwardly. The actual direction of z_{\pm} is assumed to be unimportant, provided that it is in the plane perpendicular to $\hat{\mathbf{b}}$ and that only low-frequency perturbations are relevant for the heating and acceleration of the plasma. Hence, we treat z_{\pm} as scalars. The Alfvén speed along the field line is $V_a(s) = B/\sqrt{4\pi\rho}$. With R_1^{\pm} and R_2^{\pm} respectively, we indicate the WKB and reflection terms, which are related to the large scale gradients. λ_{\odot} is the turbulence correlation scale at the solar surface. Thus the heating function H (de Karman and Howarth, 1938; Matthaeus *et al.*, 2004), p_w and R_s (Usmanov *et al.*, 2011; Usmanov, Goldstein, and Matthaeus, 2012) can all be expressed in terms of z_{\pm} . We are allowed to specify temperature and density at the lower boundary because the solar wind is subsonic there. However, the velocity must be determined by solving the 1D gas characteristic equations. Since the upper boundary is placed beyond all critical points, the characteristic equations are used for all variables. The amplitude of the outward-propagating (from the Sun) wave is imposed in the z_{\pm} equations.

Lionello *et al.* (2014b) used the model to explore the parameter space of λ_{\odot} and z_+^{\odot} (z_+ at the solar surface) in a radial field line to determine the plasma speed, density, and temperature at 1 AU. Lionello *et al.* (2014a) calculated instead solar wind solutions at different latitudes along open flux tubes of the magnetic field described in Banaszekiewicz, Axford, and McKenzie (1998). In the present work, in parallel with the HD equations, we use U , T , and n_e to evolve the fractional charge states of minor ions according to the model of Shen

et al. (2015):

$$\frac{\partial {}_Z F^i}{\partial t} + U \frac{\partial}{\partial s} {}_Z F^i = n_e [{}_Z C^{i-1} {}_Z F^{i-1} - ({}_Z C^i + {}_Z R^{i-1}) {}_Z F^i + {}_Z R^i {}_Z F^{i+1}]. \quad (9)$$

For an element with atomic number Z , ${}_Z F^i(s)$ indicates the fraction of ion $i + (i = 0, Z)$ in respect of the total at a grid point:

$$\sum_{i=0}^Z {}_Z F^i = 1. \quad (10)$$

For each element, the ion fractions are coupled through the ionization, ${}_Z C^i(T)$, and recombination, ${}_Z R^i(T)$, rate coefficients derived from the CHIANTI (version 7.1) atomic database (Dere *et al.*, 1997; Landi *et al.*, 2013). Although in principle the values of the ion fractions could be used to determine the radiation law function $Q(T)$ in Equation 3, they provide no feedback effects in this investigation. As initial condition, we prescribe at each point the equilibrium values of each ${}_Z F^i(s)$, which is obtained from the module of Shen *et al.* (2015). As boundary condition at $s = R_\odot$ we keep the initial, equilibrium ${}_Z F^i(R_\odot)$. At the outer boundary $s = 215 R_\odot$, since the charge states are frozen in, we set the values to be the same as those at the grid point immediately preceding, ${}_Z F^i(215 R_\odot) = {}_Z F^i(215 R_\odot - \Delta r)$.

3. Results

We calculate the fractional charge states in a parameter space study of the fast solar wind and for the magnetic field configuration of Banaszekiewicz, Axford, and McKenzie (1998). Since in either case the computed ion fractions do not match *in situ* measurements, we devise a correction for the ion outflow speed. Then we show the calculated charge states with the corrected flow.

3.1. Charge-States in a Parameter Study of the Fast Solar Wind

Using the WTD model described in Section 2, Lionello *et al.* (2014b) performed a parameter study of the fast solar wind along a radial magnetic field line. They varied λ_\odot at 5 values within $0.01 R_\odot \leq \lambda_\odot \leq 0.09 R_\odot$, with an interval $\Delta\lambda_\odot = 0.02 R_\odot$, and z_+^\ominus at 13 values equally spaced between $19 \text{ km s}^{-1} \lesssim z_+^\ominus \lesssim 42 \text{ km s}^{-1}$, the interval between each value being $\Delta z_+^\ominus \simeq 1.9 \text{ km s}^{-1}$. Not all values yielded steady-state solutions: when $\lambda_\odot = 0.01 R_\odot$, acceptable solutions were found only for $19 \text{ km s}^{-1} \lesssim z_+^\ominus \lesssim 31 \text{ km s}^{-1}$; when $\lambda_\odot = 0.03 R_\odot$, a steady-state solution was not found for $z_+^\ominus \simeq 42 \text{ km s}^{-1}$.

We have repeated the same simulations, having activated the ion charge-state evolution module for carbon, oxygen, and iron. In Figure 1 we show comparisons between results of the computation and the measurements of *Ulysses*/SWICS (Zurbuchen *et al.*, 2002) during the years 1994 and 1995, when the spacecraft performed the rapid latitude scans. Since the parameter study concerns the fast solar wind, we show measurements only for latitudes larger than 70° north or south. Each symbol along the curves represents the results of solutions with the same λ_\odot but increasing z_+^\ominus from bottom left to top right. Panel (a) has the ratio of O^{7+}/O^{6+} on the x -axis and C^{6+}/C^{5+} on the y -axis and panel (c) has the average charge state of iron, $\langle Q \rangle_{\text{Fe}}$, versus the O^{7+}/O^{6+} ratio [panels (b) and (d) will be described later]. From panel (a) it is evident that, although in some instances values of O^{7+}/O^{6+} compatible with *in situ* data are reproduced, there are no solutions that can simultaneously match the

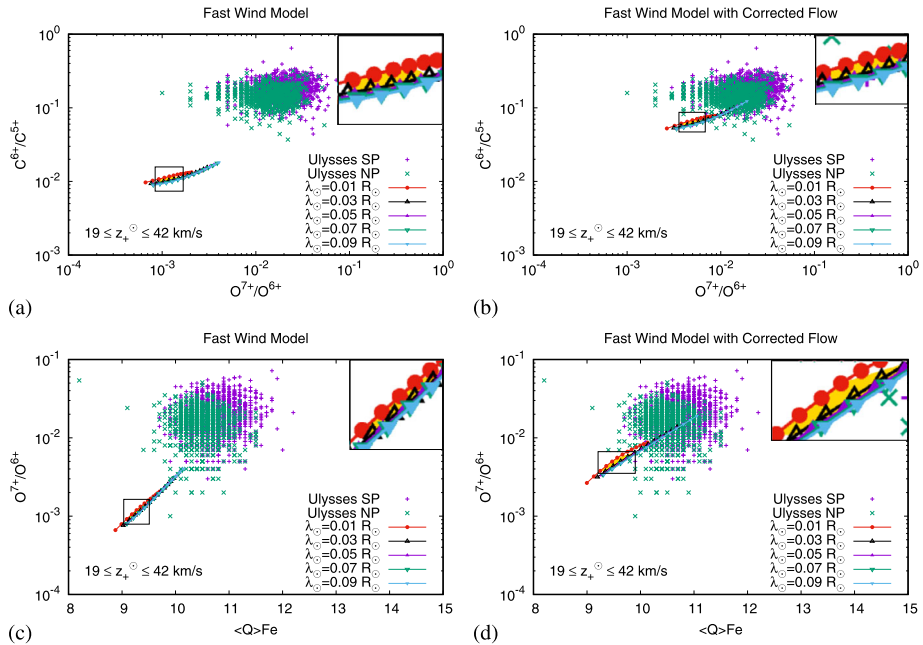


Figure 1 The ion charge states at 1 AU in the parameter study of the solar wind in WTD model of Lionello *et al.* (2014b) compared with the measurements of *Ulysses* at latitudes $|\phi| \geq 70^\circ$ during 1994–1995. Values from simulations with the same λ_\odot are grouped along curves. Along each curve a symbol indicates the calculated result. z_+^\ominus increases from bottom left to top right at 13 values equally spaced between $19 \text{ km s}^{-1} \lesssim z_+^\ominus \lesssim 42 \text{ km s}^{-1}$, the interval between each value being $\Delta z_+^\ominus \simeq 1.9 \text{ km s}^{-1}$. The thin area in gold corresponds to solutions with $630 \lesssim U \lesssim 820 \text{ km s}^{-1}$ and $1.5 \lesssim n_e \lesssim 3 \text{ cm}^{-3}$ for the plasma at 1 AU. Enlargements around the areas are provided in the upper right corners of each panel. (a) O^{7+}/O^{6+} vs. C^{6+}/C^{5+} in the original model. (b) The same as (a) with corrected flow in the evolution of the ions. (c) $\langle Q \rangle \text{Fe}$ vs. O^{7+}/O^{6+} in the original model. (d) The same as (c) with corrected flow in the evolution of the ions.

measured C^{6+}/C^{5+} and O^{7+}/O^{6+} . Panel (c) shows some superposition between measurements and calculations with the highest values of z_+^\ominus . However, as it appears from Figure 2 of Lionello *et al.* (2014b), these large z_+^\ominus yields plasma parameters at 1 AU that are not generally observed in the solar wind. On the contrary, the thin area in gold in panel (c), which corresponds to solutions with $630 \lesssim U \lesssim 820 \text{ km s}^{-1}$ and $1.5 \lesssim n_e \lesssim 3 \text{ cm}^{-3}$, does not intersect the bulk of *Ulysses* measurements.

3.2. Latitudinal Profiles of Charge-States in the Solar Wind

Lionello *et al.* (2014a) used the WTD model of Section 2 to calculate solar wind solutions along 25 magnetic field lines extracted at different latitudes between 0° and 90° from the 2D, axisymmetric, analytic model of Banaszekiewicz, Axford, and McKenzie (1998). For each flux tube, the same combination of turbulence parameters $z_+^\ominus = 54 \text{ km s}^{-1}$ and $\lambda_\odot = 0.02 R_\odot$ was employed. The computed latitudinal dependence at 1 AU of plasma wind speed, number density, temperature, and pressure (Figure 2 of Lionello *et al.*, 2014a) was found to be in qualitative agreement with the more advanced model of Cranmer, van Ballegooijen, and Edgar (2007) and within the range of *in situ* data.

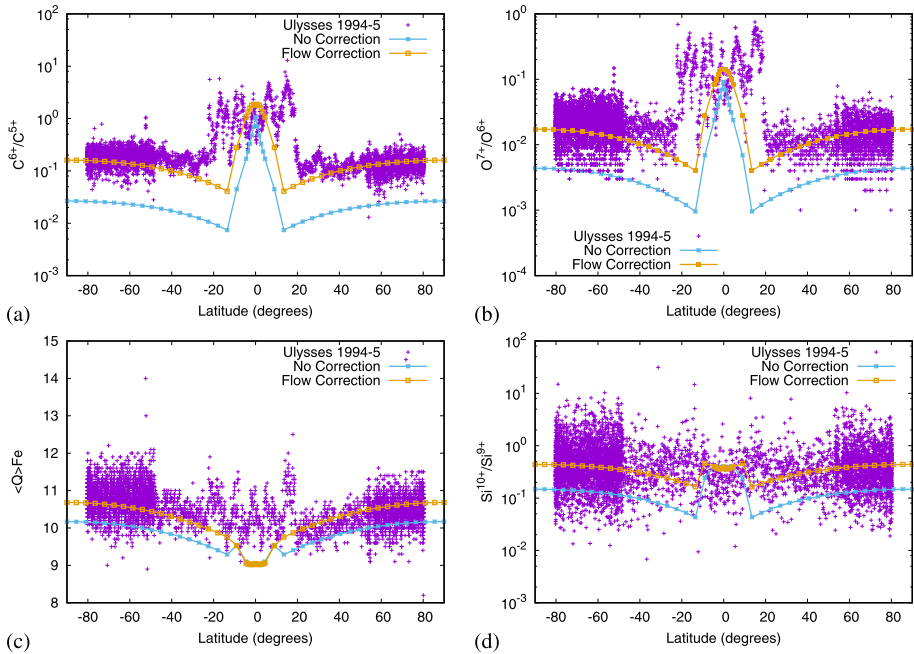


Figure 2 Latitudinal dependence of ion charge states of the solar wind at 1 AU in the WTD model of Lionello *et al.* (2014a) compared with the measurements of *Ulysses* during 1994–1995. 25 solar wind solutions (indicated with *symbols along the curves*) were calculated at latitudes between 0° and 90° along field lines of the symmetric model of Banaszkiewicz, Axford, and McKenzie (1998). The *cyan curves* are for the unmodified charge-state evolution model, the *orange curves* show the results when a correction to the flow is applied. (a) C^{6+}/C^{5+} . (b) O^{7+}/O^{6+} . (c) $\langle Q \rangle Fe$. (d) Si^{10+}/Si^{9+} .

We have also repeated the simulations of Lionello *et al.* (2014a) to calculate the charge states for carbon, oxygen, and iron. In Figure 2a we compare the latitudinal dependence of the computed C^{6+}/C^{5+} ratio (in cyan, each symbol representing a solution) with that measured by *Ulysses* during 1994–1995. Although we cannot expect agreement at low latitudes, where the charge states are affected by the properties of the equatorial streamer and possible encounters with CMEs, the results of the simulations are about one order of magnitude too low even at the poles. The calculated O^{7+}/O^{6+} ratios (in cyan) in Figure 2b are also too low. The curve of simulated average iron charge states, $\langle Q \rangle Fe$, which is depicted in cyan in Figure 2c, is at the lower limit of the measurements.

3.3. Correcting the Ion Outflow Speed

Since the results in Sections 3.1 and 3.2 show that the WTD model described in Section 2 cannot reproduce the charge states of ions in the solar wind, we have looked for possible improvements that may also be implemented in the 3D model of Mikić *et al.* (2018). One possible reason why the charge states in our model are too low is that we do not include the effect of a suprathermal electron tail in the corona that would increase the ionization coefficients (Ko *et al.*, 1996; Esser, Edgar, and Brickhouse, 1998; Cranmer, 2014). However, no conclusive evidence of such non-Maxwellian distribution has yet emerged (Cranmer, 2009). Another possibility is that a simple, one fluid model does not account for the possibility that

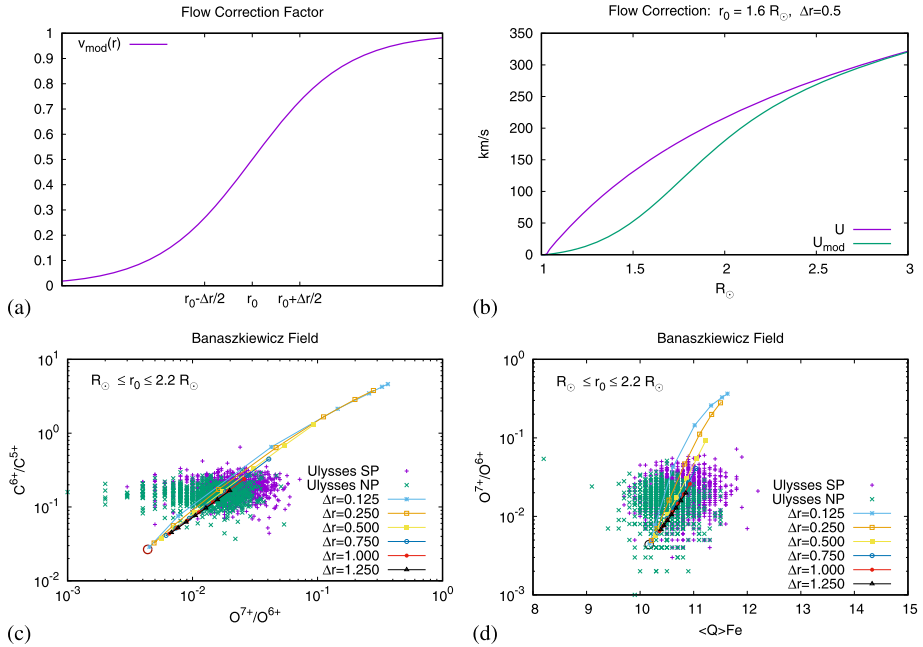


Figure 3 (a) A plot of the two-parameter (*i.e.*, Δr and r_0) function in Equation 12. (b) In purple, the solar wind speed along the polar magnetic field line of the model of Banaskiewicz, Axford, and McKenzie (1998) calculated with the WTD algorithm. In green, the speed used to advance the charge states in Equation 9 when $v_{\text{mod}}(r)$ with $\Delta r = 0.5 R_\odot$ and $r_0 = 1.6 R_\odot$ is applied to the flow as in Equation 11. (c) O^{7+}/O^{6+} vs. C^{6+}/C^{5+} at 1 AU for the same field line. The circle in the lower left corner shows the values if no correction is applied to the flow in Equation 9. Values along each curve, from bottom left to top right, represent solutions with the same Δr in $v_{\text{mod}}(r)$ and increasing r_0 , from 1 to $2.2 R_\odot$ at intervals of $0.2 R_\odot$. The curves are superimposed to the *Ulysses* measurements at latitudes $|\phi| \geq 70^\circ$ during 1994–1995. (d) The same as (c) but for $\langle Q \rangle_{\text{Fe}}$ vs. O^{7+}/O^{6+} .

ions traveling at lower speeds than electrons would spend more time in the lower corona, where they would likely reach higher charge states (Ko, Geiss, and Gloeckler, 1998). Landi *et al.* (2014) proposed a correction to the flow in the model of Cranmer, van Ballegoijen, and Edgar (2007) to have the source region located in the corona rather than in the lower atmosphere. The charge states of the solar wind were already closer to the measured ones, but still a better agreement was reached mostly due to this fact. Inspired by their work, we intend to determine a modifying factor $v_{\text{mod}}(r)$ such that when applied to $U(s)$,

$$U_{\text{mod}}(s) = v_{\text{mod}}(r)U(s), \tag{11}$$

may give a smaller ion outflow speed in the lower corona, and thus make the charge states at 1 AU as calculated in Equation 9 compatible with the *Ulysses* measurements. We choose for $v_{\text{mod}}(r)$ the following formulation:

$$v_{\text{mod}}(r) = \frac{1}{2} \left(1 + \tanh \frac{r - r_0}{\Delta r} \right), \tag{12}$$

which is based on two parameters, r_0 and Δr . As Figure 3a shows, r_0 controls where the flow is switched on and Δr is the interval over which this transition occurs. To determine

heuristically the optimal values of these parameters, we repeat the charge-state calculation for the polar field line in Section 3.2 with v_{mod} having $r_0 = 1, 1.2, 1.4, 1.6, 1.8, 2., 2.2 R_{\odot}$ and $\Delta r = 0.125, 0.25, 0.75, 1, 1.25 R_{\odot}$. Then we evaluate for each solution the values of the ratios O^{7+}/O^{6+} and C^{6+}/C^{5+} as well as $\langle Q \rangle \text{Fe}$. Finally, we select the couple $(r_0, \Delta r)$ that yields the results closest to the *Ulysses* measurements. Figures 3c and 3d show the calculated charge states, respectively, in the C^{6+}/C^{5+} vs. O^{7+}/O^{6+} and in the $\langle Q \rangle \text{Fe}$ vs. O^{7+}/O^{6+} planes. Each curve corresponds to a given Δr . The symbols along each curve represent values of r_0 increasing from the bottom left (where the charge states for the solution with no v_{mod} are indicated with circles) to top right. The values corresponding to the couple $(r_0 = 1.6 R_{\odot}, \Delta r = 0.5 R_{\odot})$ fall close to the centers of the *Ulysses* measurements. With this choice, the ion outflow speed is modified as depicted in Figure 3b. Since the ions are traveling for a longer time in the lower corona, they can reach higher charge states before being “frozen in.”

3.4. Charge States Calculations with Modified Ion Outflow Speed

We have repeated the calculations of Section 3.1 with the ion outflow speed modified with v_{mod} according to the optimal choice of parameters ($\Delta r = 0.5 R_{\odot}$ and $r_0 = 1.6 R_{\odot}$) as described in the previous subsection. The effects of the modification can be seen in Figures 1b and 1d, which are the respective counterparts of the unmodified calculations in Figures 1a and 1c. Higher charge states are reached so that now the thin areas in gold, which correspond to solar wind solutions with $630 \lesssim U \lesssim 820 \text{ km s}^{-1}$ and $1.5 \lesssim n_e \lesssim 3 \text{ cm}^{-3}$, intersect (or at least touch) the bulk of *Ulysses* measurements. Hence, solutions in these subregions have not only plasma velocity and density, but also charge-state values compatible with *in situ* measurements.

Analogously, we have recalculated the latitudinal profiles of Section 3.2 applying v_{mod} to slow down the flow of ions. The orange curves in panels (a), (b), and (c) of Figure 2, which correspond to simulations with the corrected ion outflow speed, show higher charge states being formed in comparison with the cyan curves, for which no such modification is applied. Thus, at least for the higher latitudes, the calculated charge states lie now close to the middle of the bulk of the *Ulysses* measurements.

To verify our approach, we also calculate the $\text{Si}^{10+}/\text{Si}^{9+}$ ratio, which has not been used to optimize the parameters of the v_{mod} function and for which there exist data in the *Ulysses*/SWICS archive. The resulting latitudinal profiles, with and without the ion outflow speed correction, are shown in Figure 2d superimposed to the measurements. These, due to uncertainties, span about two orders of magnitude. Although both curves fall within the bulk of the data, the profile with flow correction lies closer to the average value. This confirms that our approach is not, at least, inferior to that using the unmodified flow.

4. Conclusions

We have incorporated time-dependent fractional charge states evolution into our 1D WTD model of the solar wind. We have implemented this capability with the aim of introducing it also into our 3D MHD model of the solar corona and inner heliosphere. In fact, charge-state calculations, especially when combined with other EUV, X-ray, and white-light emission diagnostics, represent a powerful constraint on the underlying WTD MHD model. They can provide additional constraints on the correlation scale of the turbulence and the ampli-

tude of the outwardly propagating Alfvén perturbation at the solar surface. However, the charge-state percentages as calculated from the WTD model do not match the heliospheric measurements taken by *Ulysses* in 1994–1995. We have heuristically determined a correction to the ion outflow speed to be used to evolve the charge states. This yields, particularly for the polar regions, a better agreement between the calculated values and the *in situ* measurements of *Ulysses* during 1994–1995. At lower latitudes, where there are uncertainties due to possible encounters with CMEs and the configuration of the equatorial streamer, the discrepancy is larger. Comparing our work with that of Oran *et al.* (2015), we notice first the differences between their models and ours: Oran *et al.* employed a global MHD algorithm driven by a sophisticated Alfvén WTD formulation, selected field lines at different latitudes, used an external code to evaluate the charge states along the same, and compared the results with the measurements of *Ulysses* during its third polar scan of 2007. Yet, despite all these differences, their models disagreed with measurements in the same sense as ours, namely ionization rates were underpredicted. Oran *et al.* (2015) considered the same explanations we discuss in the text, but, finally, invoked suprathermal electrons as a possible, unaccounted mechanism to close the gap with observations. We have postulated a slower propagation speed for the ions. Although the ion outflow speed modification, which was inspired by that of Landi *et al.* (2014), may capture some of the physics of the ions, there are several other possible explanations for the mismatch between the calculated charge states and the observations. On the other hand, our modified ion outflow speed (Figure 3b) lies within the range of recent empirical results (Figure 4 of Abbo *et al.*, 2016), since it is already more than 300km s^{-1} at $3 R_{\odot}$. It is also possible that photoionization may yield the higher charge states measured in the solar wind. Even if Landi and Lepri (2015) found that it could be a significant factor, yet it was not sufficient to explain the discrepancy between predictions and measurements. We plan to explore this effect in future work. Moreover, the plasma density and temperature in the lower corona could also be factors of critical importance in setting the charge-state distribution of the solar wind. Although our model was shown to provide results compatible with observations (Lionello *et al.*, 2014a), we cannot categorically exclude that a different heating model could yield not only the same plasma parameters at 1 AU, but also conditions in the lower corona causing higher ionization. Needless to say, a more accurate calculation of charge states would also require multi-fluid simulations (*e.g.*, Ofman, Abbo, and Giordano, 2013) or even multi-ions simulations (*e.g.*, Byhring *et al.*, 2011). In particular, as Figure 3b of Byhring *et al.* (2011) shows, a single outflow speed for all ions is only a crude approximation. Introducing a more realistic evolution of the plasma, starting from evolving the temperature of electrons and protons separately, is a first step into this direction that will be implemented next. However, considering the end goal of our investigation is to provide accurate 3D modeling of the corona and heliosphere capable of predicting tomorrow's conditions from today's empirical data, compromises on which physical mechanisms to include next will be inevitable. They will also be acceptable only if the results can be quantitatively matched with observations.

Acknowledgements R. Lionello is grateful to Drs. Susanna Parenti and Alessandro Bemporad for providing helpful advice. We also thank the referee for constructive criticism. R. Lionello was funded through NASA Grant NNH14CK98C.

Disclosure of Potential Conflicts of Interest The authors declare that they have no conflicts of interest.

Publisher's Note Springer Nature remains neutral with regard to jurisdictional claims in published maps and institutional affiliations.

References

- Abbo, L., Ofman, L., Antiochos, S.K., Hansteen, V.H., Harra, L., Ko, Y.-K., Lapenta, G., Li, B., Riley, P., Strachan, L., von Steiger, R., Wang, Y.-M.: 2016, Slow solar wind: Observations and modeling. *Space Sci. Rev.* **201**, 55. DOI. ADS.
- Athay, R.G.: 1986, Radiation loss rates in Lyman-alpha for solar conditions. *Astrophys. J.* **308**, 975. ADS.
- Banaszkiewicz, M., Axford, W.I., McKenzie, J.F.: 1998, An analytic solar magnetic field model. *Astron. Astrophys.* **337**, 940. ADS.
- Bochsler, P.: 2002, Abundances and charge states of particles in the solar wind. *Rev. Geophys.* **38**(2), 247. DOI.
- Buergi, A., Geiss, J.: 1986, Helium and minor ions in the corona and solar wind – Dynamics and charge states. *Solar Phys.* **103**, 347. DOI. ADS.
- Byhring, H.S., Cranmer, S.R., Lie-Svendsen, Ø., Habbal, S.R., Esser, R.: 2011, Modeling iron abundance enhancements in the slow solar wind. *Astrophys. J.* **732**, 119. DOI. ADS.
- Chen, Y., Esser, R., Hu, Y.: 2003, Formation of minor-ion charge states in the fast solar wind: Roles of differential flow speeds of ions of the same element. *Astrophys. J.* **582**, 467. DOI. ADS.
- Cranmer, S.R.: 2002, Coronal holes and the high-speed solar wind. *Space Sci. Rev.* **101**, 229. ADS.
- Cranmer, S.R.: 2009, Coronal holes. *Living Rev. Solar Phys.* **6**, 3. DOI. ADS.
- Cranmer, S.R.: 2014, Suprathermal electrons in the solar corona: Can nonlocal transport explain heliospheric charge states? *Astrophys. J. Lett.* **791**, L31. DOI. ADS.
- Cranmer, S.R., van Ballegoijen, A.A., Edgar, R.J.: 2007, Self-consistent coronal heating and solar wind acceleration from anisotropic magnetohydrodynamic turbulence. *Astrophys. J. Suppl.* **171**, 520. DOI. ADS.
- de Karman, T., Howarth, L.: 1938, On the Statistical Theory of Isotropic Turbulence. *Royal Society of London Proceedings Series A* **164**, 192. DOI. ADS.
- Dere, K.P., Landi, E., Mason, H.E., Monsignori Fossi, B.C., Young, P.R.: 1997, CHIANTI – An atomic database for emission lines. *Astron. Astrophys. Suppl.* **125**, 149. ADS.
- Dmitruk, P., Milano, L.J., Matthaeus, W.H.: 2001, Wave-driven turbulent coronal heating in open field line regions: Nonlinear phenomenological model. *Astrophys. J.* **548**, 482. DOI. ADS.
- Esser, R., Edgar, R.J., Brickhouse, N.S.: 1998, High minor ion outflow speeds in the inner corona and observed ion charge states in interplanetary space. *Astrophys. J.* **498**, 448. DOI. ADS.
- Hollweg, J.V.: 1978, Some physical processes in the solar wind. *Rev. Geophys. Space Phys.* **16**, 689. ADS.
- Ko, Y.-K., Geiss, J., Gloeckler, G.: 1998, On the differential ion velocity in the inner solar corona and the observed solar wind ionic charge states. *J. Geophys. Res.* **103**, 14539. DOI. ADS.
- Ko, Y.-K., Fisk, L.A., Gloeckler, G., Geiss, J.: 1996, Limitations on suprathermal tails of electrons in the lower solar corona. *Geophys. Res. Lett.* **23**, 2785. DOI. ADS.
- Ko, Y.-K., Gloeckler, G., Cohen, C.M.S., Galvin, A.B.: 1999, Solar wind ionic charge states during the Ulysses pole-to-pole pass. *J. Geophys. Res.* **104**, 17005. DOI. ADS.
- Landi, E., Lepri, S.T.: 2015, Photoionization in the solar wind. *Astrophys. J. Lett.* **812**, L28. DOI. ADS.
- Landi, E., Young, P.R., Dere, K.P., Del Zanna, G., Mason, H.E.: 2013, CHIANTI – An atomic database for emission lines. XIII. Soft X-ray improvements and other changes. *Astrophys. J.* **763**, 86. DOI. ADS.
- Landi, E., Oran, R., Lepri, S.T., Zurbuchen, T.H., Fisk, L.A., van der Holst, B.: 2014, Charge state evolution in the solar wind. III. Model comparison with observations. *Astrophys. J.* **790**, 111. DOI. ADS.
- Lionello, R., Velli, M., Downs, C., Linker, J.A., Mikić, Z.: 2014a, Application of a solar wind model driven by turbulence dissipation to a 2D magnetic field configuration. *Astrophys. J.* **796**, 111. DOI. ADS.
- Lionello, R., Velli, M., Downs, C., Linker, J.A., Mikić, Z., Verdini, A.: 2014b, Validating a time-dependent turbulence-driven model of the solar wind. *Astrophys. J.* **784**, 120. DOI. ADS.
- Matthaeus, W.H., Minnie, J., Breech, B., Parhi, S., Bieber, J.W., Oughton, S.: 2004, Transport of cross helicity and radial evolution of Alfvénicity in the solar wind. *Geophys. Res. Lett.* **31**, 12803. DOI. ADS.
- Mikić, Z., Linker, J.A., Schnack, D.D., Lionello, R., Tarditi, A.: 1999, Magnetohydrodynamic modeling of the global solar corona. *Phys. Plasmas* **6**, 2217. ADS.
- Mikić, Z., Downs, C., Linker, J.A., Caplan, R.M., Mackay, D.H., Upton, L.A., Riley, P., Lionello, R., Török, T., Titov, V.S., Wijaya, J., Druckmüller, M., Pasachoff, J.M., Carlos, W.: 2018, Predicting the corona for the 21 August 2017 total solar eclipse. *Nat. Astron.* DOI. ADS.
- Ofman, L., Abbo, L., Giordano, S.: 2013, Observations and models of slow solar wind with Mg⁹⁺ ions in quiescent streamers. *Astrophys. J.* **762**, 18. DOI. ADS.
- Oran, R., Landi, E., van der Holst, B., Lepri, S.T., Vásquez, A.M., Nuevo, F.A., Frazin, R., Manchester, W., Sokolov, I., Gombosi, T.I.: 2015, A steady-state picture of solar wind acceleration and charge state composition derived from a global wave-driven MHD model. *Astrophys. J.* **806**, 55. DOI. ADS.
- Shen, C., Raymond, J.C., Murphy, N.A., Lin, J.: 2015, A Lagrangian scheme for time-dependent ionization in simulations of astrophysical plasmas. *Astron. Comput.* **12**, 1. DOI. ADS.

- Usmanov, A.V., Goldstein, M.L., Matthaeus, W.H.: 2012, Three-dimensional magnetohydrodynamic modeling of the solar wind including pickup protons and turbulence transport. *Astrophys. J.* **754**, 40. DOI. ADS.
- Usmanov, A.V., Matthaeus, W.H., Breech, B.A., Goldstein, M.L.: 2011, Solar wind modeling with turbulence transport and heating. *Astrophys. J.* **727**, 84. DOI. ADS.
- Verdini, A., Velli, M., Matthaeus, W.H., Oughton, S., Dmitruk, P.: 2010, A turbulence-driven model for heating and acceleration of the fast wind in coronal holes. *Astrophys. J. Lett.* **708**, L116. DOI. ADS.
- Zurbuchen, T.H., Fisk, L.A., Gloeckler, G., von Steiger, R.: 2002, The solar wind composition throughout the solar cycle: A continuum of dynamic states. *Geophys. Res. Lett.* **29**, 1352. DOI. ADS.